New Journal of Physics
The open access journal at the forefront of physics

Deutsche Physikalische Gesellschaft DPG IOP Institute of Physics

Dislocation-induced electronic states and point-defect atmospheres evidenced by electron energy loss imaging

To cite this article: U Bangert *et al* 2004 *New J. Phys.* **6** 184

View the article online for updates and enhancements.

Related content

- Nanometrology Using the Transmission Electron Microscope: Spectroscopy
V Stolojan
- Vacancy clusters, dislocations and brown colouration in diamond
U Bangert, R Barnes, M H Gass et al.
- Calculated and experimental low-loss EEL spectra of dislocations in diamond andGaN
R Jones, C J Fall, A Gutiérrez-Sosa et al.

Recent citations

- Surface-state dependent optical properties of OH-, F-, and H-terminated 4H-SiC quantum dots
Marzaini Rashid *et al*
- The Role of Edge Dislocations on the Red Luminescence of ZnO Films Deposited by RF-Sputtering
Rocío Félix *et al*
- Optical study of defects in thick undoped CVD synthetic diamond layers
Bert Willems *et al*

This content was downloaded from IP address 137.250.100.48 on 16/05/2018 at 16:04

New Journal of Physics
The open–access journal for physics

Dislocation-induced electronic states and point-defect atmospheres evidenced by electron energy loss imaging

U Bangert[1], A J Harvey[1], R Jones[2], C J Fall[2], A T Blumenau[2,3], R Briddon[4], M Schreck[5] and F Hörmann[5]

[1] Department of Physics, UMIST, Manchester M60 1QD, UK
[2] School of Physics, University of Exeter, EX4 4QL, UK
[3] Theoretische Physik, Universität Paderborn, D-33098 Paderborn, Germany
[4] Department of Physics, Newcastle upon Tyne, Newcastle NE1 7RU, UK
[5] Universität Augsburg, Institut für Physik, D-86135, Germany
E-mail: ursel.bangert@umist.ac.uk

New Journal of Physics **6** (2004) 184
Received 15 September 2004
Published 30 November 2004
Online at http://www.njp.org/
doi:10.1088/1367-2630/6/1/184

Abstract. Electronic band gap states connected with individual dislocations in diamond and GaN are revealed, using highly spatially resolved electron energy loss (EEL) spectrum mapping. Comparison with calculations of low EEL spectra from first-principle methods allows the identification of the joint density of states of different dislocation core types. Also presented is evidence for instances where point defects/impurities have accumulated in the strain field or segregated to the core of dislocations.

Contents

1. Introduction	**2**
2. Experimental setup	**2**
3. Electronic states at dislocations in diamond	**3**
4. Dislocation-related electronic states in GaN	**6**
5. Conclusion	**9**
References	**10**

PII: S1367-2630(04)86464-4
1367-2630/04/010184+10$30.00
© IOP Publishing Ltd and Deutsche Physikalische Gesellschaft

1. Introduction

The electronic structure of extended defects in semiconductors, in spite of substantial effort, is still in general not understood. Although there is substantial evidence that defects, such as grain boundaries and dislocations, influence the optical and electrical behaviour of materials, there are severe problems in distinguishing the effects arising purely from the extended defects or from point defects, which have aggregated in the vicinity of extended defects. Two long-standing and unresolved issues involving dislocations are given as example: (i) the common brown colouration found in most natural diamonds is believed to be associated with dislocations and makes the diamond of little value to the gem trade. However, a high temperature treatment can transform a diamond into a colourless gem [1], and this may represent a transformation of a dislocation core, eliminating metastable electrically active sp_2-bonded carbon core atoms [2]; (ii) the effect of dislocations on the long-term performance of light emitting devices, e.g., blue GaN-based lasers is still not known. A number of theoretical approaches to determine the electronic effects of dislocations have been undertaken [3]–[6]; these remain to be tested by experiment. Most of the experimental evidence to date comes from measurements, which are indirect, let alone spatially resolved, so that one cannot assign a particular effect to an individual dislocation.

With scanned probe electron energy loss spectroscopy (EELS) a spatial resolution of <10 nm can be achieved, and because the spectroscopy is performed in conjunction with microstructural imaging, it is one of the few experimental techniques to give direct information about electronic levels associated with dislocations. For this, EELS is usually carried out in a scanning transmission electron microscope (STEM), where a highly localized probe excites electrons from filled into unfilled states. The recent advent of cold field emission gun STEMs (cold FEG STEM) with high mechanical and energy stability and a monochromacity of 0.3 eV has made spectroscopy of sub-nm size features possible.

2. Experimental setup

The instrument used in this investigation is a VG601 cold FEG STEM, operated at 100 keV. The probe size was typically 1 nm. Technical details are given in [17]. It should be noted that high spectrometer dispersions (0.01 eV channel^{-1}) were used, which allowed electron energy loss (EEL) features to be monitored at energy losses as low as 2 eV. This is a crucial development as it now allows the monitoring of electronic excitations from the highest occupied bands to empty ones lying only about 2 eV higher in energy. Thus, for the first time, we have the opportunity to explore the levels of extended defects in wide-band-gap materials. The EEL technique employed here is aided by a new generation of CCD-based detectors and advanced software, which allows the acquisition of spectrum images or spectrum maps. In contrast to conventionally obtained results, i.e., via single spectrum EELS, the spectrum-mapping technique helps to reveal subtle changes involved with electronic states at dislocations, because systematic changes in the EEL spectra show up notably in a spectrum map, and they can be directly related with microstructural features. After a spectrum map was taken the area was carefully inspected for radiation damage. If changes in the microstructure were visible, the spectrum map was discarded. Sample regions of >60 nm thickness usually showed no changes and hence no indication for radiation damage.

It should further be noted that the spectrum processing was kept to a minimum, and only the zero-loss peak was subtracted from the spectra, although for purposes of electronic structure investigations it would have been desirable to extract the dielectric function. However, there are no routines to obtain the latter for EELs below 10 eV without introducing severe artifacts. Therefore, a ‘bottom-up’ approach was employed whereby the dielectric function was calculated from first-principle methods and then used to obtain model EEL spectra, which were compared with the experimental spectra.

The influence of structural defects, such as dislocations, on the electrical and optical properties of a material is determined essentially by the nature of the atomic bonding at the dislocation core. Self-consistent *ab initio* simulations within the local density approximation (LDA) to density functional theory are to date a successful approach to model energy levels associated with dislocations. On the basis of these energy calculations EEL spectra can then be simulated, and subsequently compared with experimental spectra. Energy band structure calculations of dislocations within the LDA using the AIMPRO code [7] have been described in detail elsewhere [6, 8]. The low-loss part of the EEL signal results from the scattering of the primary electron with secondary valence electrons, which undergo a transition to empty conduction or gap states. The signal obtained experimentally is representative of $-\mathrm{Im}\,\varepsilon(E)^{-1}$, where $\varepsilon = \varepsilon_1 + \varepsilon_2$ is the dielectric function and E the energy loss. We calculate the imaginary part of the dielectric function in the long-wavelength dipole approximation by summing transition matrix elements over all the bands and over the Brillouin zone:

$$\varepsilon_2^l = \frac{(4\pi e^2)}{\Omega} \sum_{c,v,k} |\langle \Psi_k^c | r^l | \Psi_k^v \rangle|^2 \delta(E_k^c - E_k^v - E),$$

where Ω is the unit cell volume, and $|\Psi_k^{v,c}\rangle$ are valence and conduction band states with energies $E^{v,c}$, respectively. The real part ε_1 and hence ε is obtained via Kramers–Kroenig transformation. The dielectric function depends only on the orientation of the electric field associated with the electron beam through the orientation r. Consequently, low EEL spectra were calculated for various orientations l of the electron beam. They represent a unique fingerprint of the energy band structure.

3. Electronic states at dislocations in diamond

Extended defects in un-doped CVD diamond [9, 10] and natural type II diamond [11, 12] have particularly been correlated with band-A cathodoluminescence at 2.8–2.9 eV, which has been associated with carbon atoms in reduced coordination [10]. Furthermore, the absorption edge EEL studies suggest that the colour of natural brown diamond is linked to sp_2-bonding at dislocation cores [13]. Interestingly, the above-mentioned LDA calculations of pure dislocation cores in diamond do not yield EEL spectra with transitions deep in the band gap. In fact, dislocations of the screw/glide type only show the enhanced joint density of states (JDOS) in the lower conduction band (see figures 1(d) and (f)). However, the band structure of metastable dislocations of the shuffle type shows a pronounced peak above mid-gap, a fingerprint of sp_2-bonding (see figure 1(e)). However, not all diamonds, especially those that have been well annealed, are expected to contain shuffle segments. The theoretical low-EEL spectrum for various dislocations in diamond is shown in figures 1(d)–(f) [8]. We note additional loss in an energy window set between 5 and 8 eV over the loss found in bulk material. The additional intensity

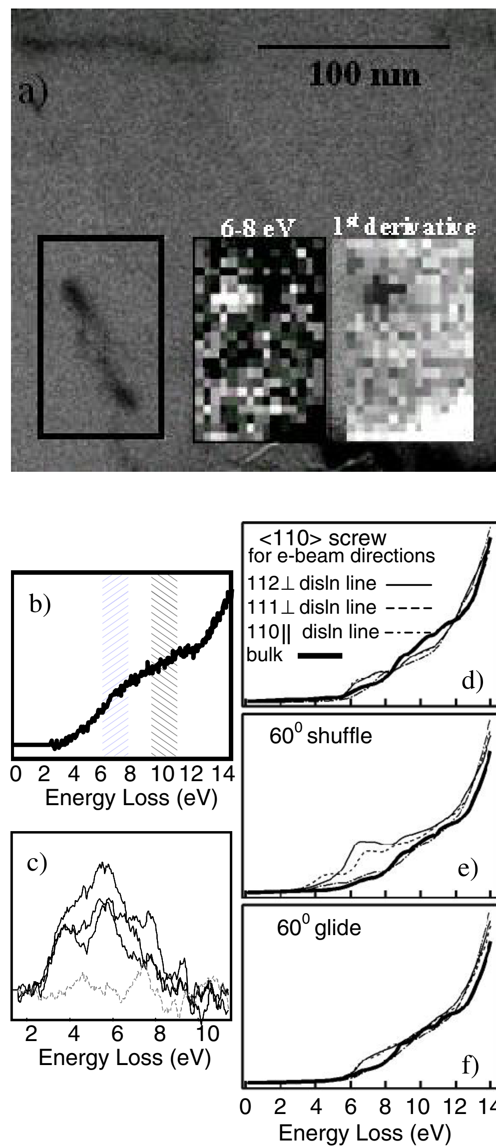

Figure 1. (a) Bright field STEM image of CVD diamond film showing inclined defect (left frame) with pixel map of the normalized integrated counts in the energy window 6–8 eV in each respective EEL spectrum (middle frame) and the integrated value of the normalized first derivative in the same energy window (right frame). (b) Experimental zero-loss extracted low loss spectrum. Windows for the construction of the intensity ratio map in (a) are indicated. (c) Scaled spectra (solid lines) showing the difference between EEL spectra from pixels of the dislocation node (white and black pixel areas in the pixel maps in (a), of the 6–8 eV window and the first derivative, respectively) and perfect bulk. The grey, broken line shows the difference between different bulk EEL spectra. (d)–(f) Show calculated low-loss spectra for various perfect dislocations in diamond together with diamond bulk spectra. Calculations are carried out for E-field polarizations parallel and perpendicular to the dislocation line.

loss disappears in an energy window between 8 and 10 eV. In the case of the screw dislocation, the EEL intensity for the bulk even exceeds that due to the dislocation. Figure 1(a) shows the image of an inclined dislocation in a single crystalline CVD diamond film. It exhibits two nodes between which it has split. Dislocation nodes are very common in single crystal diamond. If the experimental data contain the conclusions drawn from the theory above, then a contrast enhancement at the dislocation should be observed, when a map is constructed in the following way: a spectrum image was acquired by stepping the electron beam in a 15×22 pixel array over the area (indicated by the frame) across the dislocation, i.e., a low-EEL spectrum was taken in each pixel. The zero-loss peak was extracted from each spectrum via subtraction, after its tail had been fitted by a power-law function. Two energy windows were then defined in the above energy ranges in the zero-loss extracted spectra (see figure 1(b)). The values of the integrated counts in both windows were divided by each other for each spectrum, and the value of this ratio was then displayed as a grey value map. The intensity map in the image in figure 1(a) (6–8 eV) delineates the region around the upper dislocation node as a patch of brighter contrast. (This node lies near the electron beam entrance surface. The absence of a similar contrast enhancement at the lower node is thought to be due to a decrease in the sensitivity of the electron probe for features lying at the sample exit surface.)

A map can also be constructed of the relative gradient of the spectra. This was achieved by calculating the first derivative of each EEL spectrum and by normalizing this derivative function to the spectrum intensity at each respective energy value. The gradient is expected to be smaller in the energy window 5–8 eV at the dislocation compared with the bulk. The pixel map in figure 1(a) (1st derivative) shows the node accordingly, as a patch of reduced intensity. The energy spectrum of the dislocation cannot be determined from the intensity maps alone. In order to compare the spectral shape with the calculations, spectra from the dislocation node were extracted and a bulk spectrum was subtracted. The bulk spectrum was scaled so as to make the difference with the dislocation spectrum zero in the region above 10 eV, where dislocation and bulk spectra are predicted to become similar. Experimental difference spectra extracted from three pixels in the dislocation node (figure 1(c)) give evidence for the enhanced JDOS between 4 and 8 eV. We have obtained spectra similar to this for many dislocations, and the energy regime for the excess states is in accordance with the calculations for the shuffle-type geometry. It has to be pointed out that these states do not seem to be distributed along the entire dislocation line. A spectral distribution similar to this in figure 1(c)) has been consistently observed in regions of nodes. It may be the case, therefore, that these states are not innate to the shuffle core geometry, but arise due to the general existence of sp_2 bonds in the vicinity of the dislocation core.

A point worth noting is the spatial resolution that can be obtained in the low EELS measurements. According to the classical theory, the cut-off impact parameter for scattering can be approximated by v/w, where v is the velocity of the electron and w the frequency of the energy loss. Muller and Silcox [14] find that quantum mechanical treatment leads to quantitative agreement for the semi-classical limit. Based on this, for our case, for losses below 10 eV and a 100 keV primary beam the cut-off range is approximately 10 nm. Hence, this is the localization that can be expected for the low EELS with a centred collector aperture. The patch of bright contrast occurring at the dislocation node is diffuse and 2–3 pixels, i.e. at least 20 nm, in diameter. This suggests that the scattering might not solely arise from dislocation core states, but from scattering centres surrounding it. As mentioned before, the excess intensity peaking at around 6 eV in the shuffle dislocation spectra arises from the incorporation of sp_2 bonds. Such bonds, however, might not only be due to the dislocation core, but also have a more general cause. The

sp_2 defect is common and easily produced by any type of lattice disorder in diamond, and will for example, occur when point defects aggregate. Such defects need to be stabilized, and this can happen in the strain field of dislocations. Dislocation nodes have high strain fields, and hence they are likely to attract point defects.

4. Dislocation-related electronic states in GaN

Turning to GaN, the calculated spectra of all dislocation types and core structures exhibit gap states [6]. A significant role is also attributed to the interaction of point defects, i.e., impurities and vacancies, with extended defects: it has been previously reported that V_{Ga} may be trapped in the strain field of dislocations [1] and recent experiments have shown that V_{Ga} are indeed trapped at grain boundaries and hence presumably at edge dislocations [15]. Calculations incorporating point-defect geometries at the dislocation cores have been carried out for the V_{Ga}–O complex [16], but direct evidence has not been forth coming. In our study, we examine undoped MOCVD-grown GaN in cross-sectional geometry, where the electron beam is perpendicular to the *c*-axis. We found previously [17] that this geometry is not disadvantageous over the plan view, in which the electron beam propagates along the dislocation core; indeed, effects arising from the contamination/oxidation of the dislocation core are largely minimized in the cross-sectional geometry. The same individual dislocations, on which the EEL analysis was carried out in the STEM, had also undergone Burgers' vector analysis, e.g. by setting up appropriate two-beam conditions, in a conventional transmission electron microscope (CM20).

In figure 2(a), we show a STEM bright field image of a screw dislocation. Intensity ratio maps using a 0.4 eV wide lower-energy window, which we have stepped from below to above the conduction band edge revealed enhanced intensity at the dislocation between 3 and 4 eV (see grey level map in figure 2(a)). The energy states at dislocations in GaN are relatively closer to the band edge than in diamond. The chosen width of the energy window might therefore not separate these states sufficiently from the conduction band density of states and, therefore, the relative increase of states at dislocations might not be optimally revealed in energy window ratio maps. To make sure that our results obtained in the grey level map in figure 2(a) are correct, we have carried out an additional alternative evaluation and displayed the result similarly as grey value contrast map. The alternative approach involves fitting a Gaussian distribution function to the rising portion of the conduction band density of states in GaN. The fit was carried out for each spectrum in the spectrum map taken of the framed region in figure 2(a). Extra states in the band gap were then revealed by an increase in the FWHM of the Gaussian fit function. Secondly, the gap states affected the overall goodness of fit, resulting in significant residual intensity at around the band gap energy after the subtraction of the Gaussian fit function from the spectrum. In grey value maps (i.e., assigning values of increasing brightness to values of increasing FWHM or residual signal intensity), the latter evaluation methods revealed the same line of bright contrast along the dislocation line in the pre-band-edge-energy region, as the contrast map in figure 2(a) obtained via the energy window ratio method. This confirms that the dislocation possesses states within the gap. We can furthermore deduce that the extra scattering events arise from states directly at the dislocation core as the contrast line is sufficiently narrow: it is confined to the width of one pixel (approximately 6 nm), which, interestingly is even less than the rule of thumb localization for a scattering event in the 3 eV regime. Figure 2(c) shows the theoretical spectrum of a full core screw dislocation together with a spectrum of the perfect GaN bulk [6]. The experimental

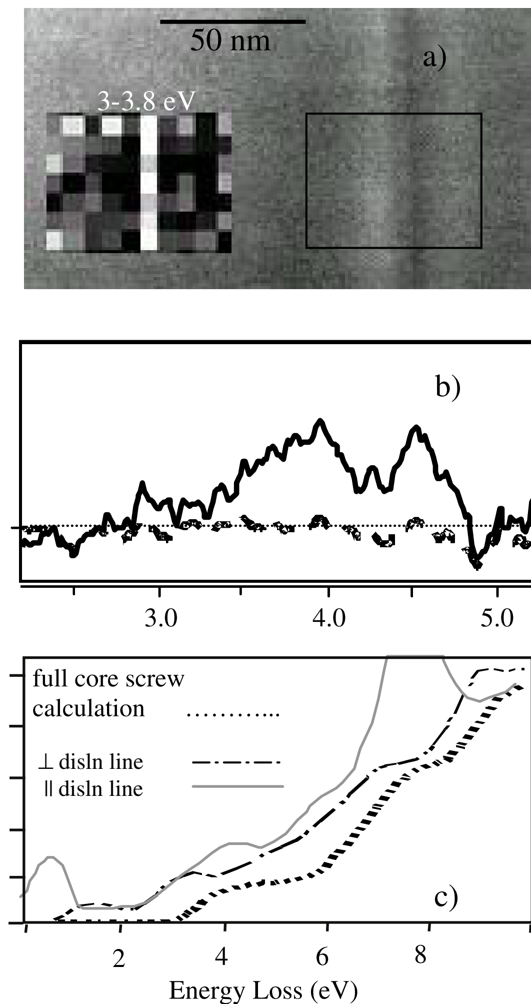

Figure 2. (a) Bright field STEM image showing a section of a threading screw dislocation (running from top to bottom) in GaN. A map of the normalized integrated counts in the energy window 3–3.8 eV is shown in the left-hand side frame, the right-hand side frame is the region in which the spectrum map for this was taken. (b) Scaled spectrum (solid line) showing the difference between summed EEL spectra from pixels of the dislocation line and summed spectra of the perfect bulk. The broken line shows the difference spectrum between bulk EEL spectra from different positions. (c) Calculated spectra for a full core screw dislocation and for bulk GaN for E-field polarizations parallel and perpendicular to the dislocation line.

spectrum (solid line) shown in figure 2(b) is a difference spectrum obtained by subtracting a sum of 'bulk' spectra, which were extracted from pixels away from the dislocation line, from a sum of 'dislocation' spectra of pixels at the dislocation line. The spectra were scaled to make the difference zero at around 5 eV. A peak can be seen at around 4 eV, and the distribution is skewed towards lower energies. The difference between the screw and the bulk spectra of the calculated spectra in figure 2(c), when scaled to zero at around 5 eV, reveals a peak at 3.5 eV, if contributions of E-field polarizations, both, perpendicular and parallel to the dislocation line,

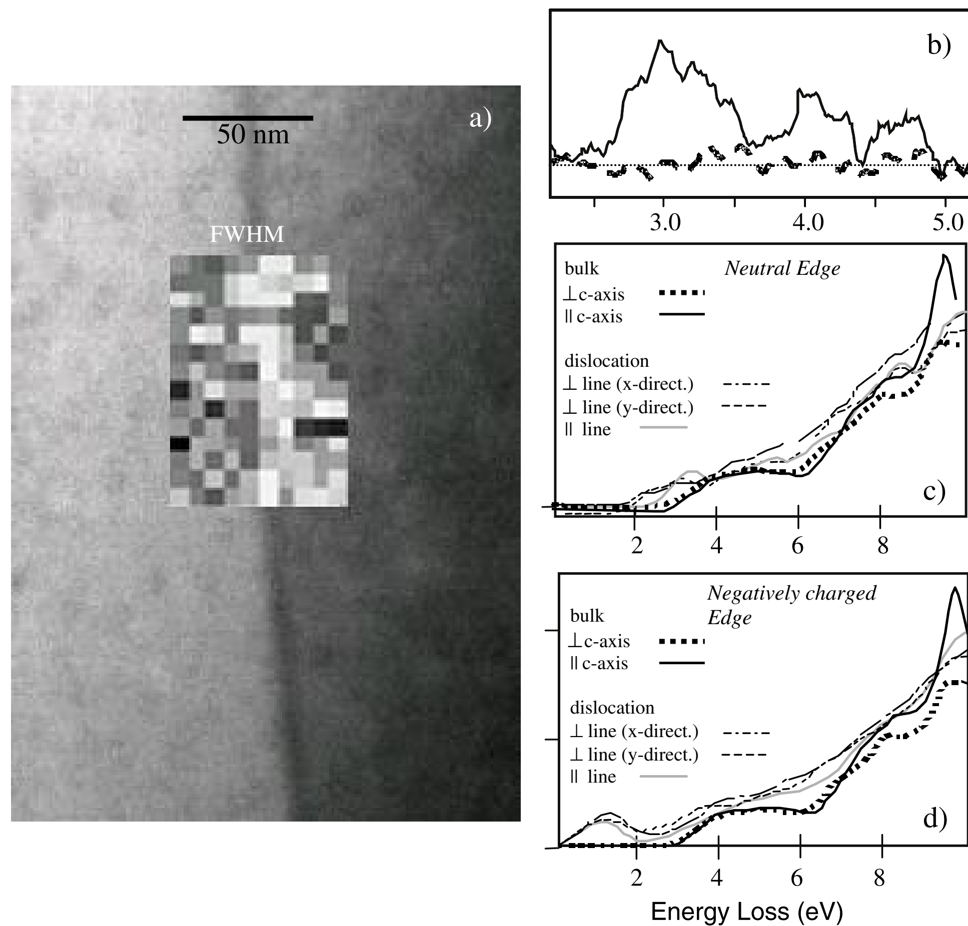

Figure 3. (a) Bright-field STEM image of a threading-edge dislocation in GaN (running from top to bottom). The grey value map of the FWHM (larger values are assigned lighter shades) of the Gaussian fit function to the rise of the conduction band density is overlaid on the image in the exact position, where the corresponding spectrum map was taken. The intensity distribution here is in stark contrast to the narrow line of the screw dislocation in figure 2. (b) Scaled spectrum (solid line) showing the difference between summed EEL spectra from pixels of the dislocation core region and summed spectra of the perfect bulk. The broken line shows the difference spectrum of bulk EEL spectra from different positions. (c), (d) Calculated EEL spectra of edge dislocations and bulk GaN.

are taken into account. There is also a tail towards lower energies. The discrepancy in the peak energy between theory and experiment are not surprising: the experimental difference spectrum is strongly affected by the detection limit at low losses, and hence will be modified by a weighting function, which reflects this. As the detection capability deteriorates significantly below 2.5 eV, the experimental difference spectrum tends to zero below this energy, resulting in a shift of the peak maximum towards higher energies than in the theoretical difference spectrum. Also shown (dashed line) in figure 2(b) is a difference spectrum of bulk spectra taken at different points, which gives a featureless intensity distribution as would be expected.

Difference spectra similar to those in figure 2(b) are shown for a threading edge dislocation in figure 3(b). Threading edge dislocation cores are believed to be negatively charged in n-material

[4, 5, 15, 18, 19] and negative, neutral or positive charge can arise in semi-insulating (Zn-doped) and p-type (Mg) material [20]. In the experimental EEL spectra, scattering intensity below 2 eV cannot at present be accurately extracted, so it would be difficult to detect the deep gap state found theoretically for a negatively charged edge dislocation (figure 3(d)). However, the intensity distribution of the experimental edge dislocation difference spectrum (figure 3(b)) is distinctively different from that of the screw dislocation. The difference spectrum was obtained by subtracting a sum of GaN bulk spectra from a sum of spectra extracted from pixels of the dislocation core, scaled such that the difference between the spectra was zero at 5 eV, as in the previous example of the screw dislocation. Here, the distribution of states is drawn out to lower energies and peaks at around 3 eV. Difference spectra constructed from theoretical edge dislocation and bulk spectra peak at 2.8–3 eV. Taking the detection limit into account, the experimental difference spectra reflect the intensity distribution of the theoretical spectra (figures 3(c) and (d)) in the energy region 2–5 eV reasonably well.

An image of a threading edge dislocation in GaN with overlaid intensity map is shown in figure 3(a)). The intensity map here was obtained by displaying the FWHM of the Gaussian-fit function to the rise of the conduction band density of states as grey value. The band of lighter grey values is notably more diffuse than in the case of the screw dislocation in figure 2(a), i.e., it extends over a distance of >20 nm away from the dislocation core. This strongly suggests that the enhanced JDOS in the vicinity of the dislocation might arise from point defects/impurities accumulated in the strain field of the dislocation or segregated to the core. Previous theoretical modelling [16] of a variety of vacancy-oxygen defects trapped near or at the core of an edge dislocation has shown that these defects have a wide energy distribution, extending to mid gap. This might also be partially reflected in the experimental difference spectra in figure 3(b), even if they are taken of the dislocation core region. The 'poor' localization of scattering events in low loss means that the JDOS within a radius of some 10 nm will contribute to the spectra at the core.

5. Conclusion

Results of mapping EEL distributions in a dedicated STEM of regions containing extended defects in GaN and diamond are presented. Maps of the scattering intensity in characteristic energy windows, and of the FWHM of Gaussians fitted to the intensity rise at the band gap, give direct information about the existence and spatial distribution of electronic band gap states at dislocations. So, for example, the distribution of the scattering intensity below band gap revealed an enhancement in the JDOS for a screw dislocation in GaN, which is confined to the dislocation core, whereas in the case of an edge dislocation it extends more than 20 nm away from the core. The spatial extent in the JDOS was explained by impurity/point defect segregation in the vicinity of the edge dislocation.

Similarly, point-defect aggregation in dislocation strain fields, specifically at dislocation nodes, can be suggested from scattering intensity maps obtained for diamond.

Electron energy low loss spectra extracted at dislocations from the spectrum maps reveal features in good agreement with spectra from first-principle calculations. Comparing experimental and calculated EEL spectra of a screw and an edge dislocation core in GaN at energies 2–5 eV revealed the characteristic JDOS of each respective dislocation type. In diamond, a common characteristic of extended defect spectra is an enhancement of the JDOS around 6 eV, which is an indicator of sp_2-bonded carbon.

References

[1] Collins A T, Kanda H and Kitawaki H 2000 *Diamond Relat. Mater.* **9** 113
[2] Blumenau A T, Heggie M I, Fall C J, Jones R and Frauenheim T 2002 *Phys. Rev.* B **65** 205205
[3] Elsner J, Jones R, Sitch P K, Porezag V D, Elstner M, Frauenheim T, Heggie M I, Öberg S and Briddon P R 1997 *Phys. Rev. Lett.* **79** 3672
[4] Wright A F and Grossner U 1998 *Appl. Phys. Lett.* **73** 2751
[5] Leung K, Wright A F and Stechel E B 1999 *Appl. Phys. Lett.* **74** 2495
[6] Fall C J, Jones R, Briddon P R, Blumenau A T, Frauenheim T and Heggie M I 2002 *Phys. Rev.* B **65** 245304
[7] Briddon P R and Jones R 2000 *Phys. Status Solidi* b **217** 131
[8] Fall C J, Jones R, Briddon P R, Blumenau A T, Frauenheim T, Gutierrez-Sosa A, Bangert U, Mora A E, Steeds J W and Butler J E 2002 *Phys. Rev.* B **65** 205206
[9] Ruan J, Kobashi K and Choyke W J 1992 *Appl. Phys. Lett.* **60** 3138
[10] Takeuchi D *et al* 2001 *Phys. Rev.* B **63** 245328
[11] Hanley P L, Kiflawi I and Lang A R 1977 *Phil. Trans. R. Soc.* A **284** 329
[12] Kiflawi I and Lang A R 1974 *Phil. Mag.* **30** 219
[13] Kolodzie A T and Bleloch A L 2003 *Phys. Conf. Ser.* **179** 319
[14] Muller D A and Silcox J 1995 *Ultramicroscopy* **59** 195
[15] Saarinen K 2003 *ONR Workshop* unpublished
[16] Elsner J, Jones R, Heggie M I, Sitch P K, Haugk M, Frauenheim T, Öberg S and Briddon P R 1998 *Phys. Rev.* B **58** 12571
[17] Bangert U, Gutierrez-Sosa A, Harvey A J, Jones R and Fall C J 2002 *J. Appl. Phys.* **93** 2728
[18] Cherns D 2003 *ONR Workshop* unpublished
[19] Cai J and Ponce F A 2002 *Phys. Status Solidi* a **192** 407
[20] Srinivasan S, Cai J, Contreras O, Ponce F A, Look D C and Molnar R J 2002 *Phys. Status Solidi* c **0** 508